Journal of Human Evolution 90 (2016) 120–134

Contents lists available at ScienceDirect

Journal of Human Evolution

journal homepage: www.elsevier.com/locate/jhevol

Cranial vault thickness in primates: *Homo erectus* does not have uniquely thick vault bones

Lynn E. Copes*, [1], William H. Kimbel

Institute of Human Origins and School of Human Evolution and Social Change, Arizona State University, PO Box 874101, Tempe, AZ 85287-4101, USA

ARTICLE INFO

Article history:
Received 15 January 2015
Accepted 31 August 2015
Available online 1 December 2015

Keywords:
Allometry
Homo erectus
CVT
Residuals
Diploë
Skull
Autapomorphy

ABSTRACT

Extremely thick cranial vaults have been noted as a diagnostic characteristic of *Homo erectus* since the first fossil of the species was identified, but relatively little work has been done on elucidating its etiology or variation across fossils, living humans, or extant non-human primates. Cranial vault thickness (CVT) is not a monolithic trait, and the responsiveness of its layers to environmental stimuli is unknown.

We obtained measurements of cranial vault thickness in fossil hominins from the literature and supplemented those data with additional measurements taken on African fossil specimens. Total CVT and the thickness of the cortical and diploë layers individually were compared to measures of CVT in extant species measured from more than 500 CT scans of human and non-human primates.

Frontal and parietal CVT in fossil primates was compared to a regression of CVT on cranial capacity calculated for extant species. Even after controlling for cranial capacity, African and Asian *H. erectus* do not have uniquely high frontal or parietal thickness residuals, either among hominins or extant primates. Extant primates with residual CVT thickness similar to or exceeding *H. erectus* (depending on the sex and bone analyzed) include *Nycticebus coucang*, *Perodicticus potto*, *Alouatta caraya*, *Lophocebus albigena*, *Galago alleni*, *Mandrillus sphinx*, and *Propithecus diadema*. However, the especially thick vaults of extant non-human primates that overlap with *H. erectus* values are composed primarily of cortical bone, while *H. erectus* and other hominins have diploë-dominated vault bones. Thus, the combination of thick vaults comprised of a thickened diploë layer may be a reliable autapomorphy for members of the genus *Homo*.

1. Introduction

In 1891, Eugene Dubois discovered, near the village of Trinil on the island of Java, the first specimen, a calotte, of the extinct hominin species that would come to be known as *Homo erectus*. Among the characters often used to diagnose the species is a thickened cranial vault (Dubois, 1937; Weidenreich, 1943; Andrews, 1984; Bilsborough and Wood, 1988; Antón, 2002, 2003), which has been considered unique among primates and even mammals (Weidenreich, 1943; Kennedy, 1991). In fact, however, because cranial vault thickness (CVT) is a composite of the thickness of each layer of vault bone (inner and outer cortical tables, sandwiching the spongy diploë), and vault bone composition across extant and extinct primates has never been thoroughly investigated, it remains unclear if a thickened cranial vault in *H. erectus* actually represents a unique trait.

Diploë and cortical bone may be functionally independent, as diploë likely responds to red-blood-cell levels and cortical bone is likely more responsive to mineral-ion levels (Kennedy, 1991). There are additional potentially important reasons to measure the thickness of the diploë layer separately from the total thickness. First, some have suggested that diploë functions to protect the brain by increasing the thickness of the vault while reducing its weight and without proportionally reducing its strength (Anzelmo et al., 2015), so it is possible that selection might act to maintain the ratio of diploë to total thickness, rather than act on absolute thickness of any single layer. Second, it has been shown that the three layers of vault are somewhat independent, with the inner table more responsive to brain growth and the outer table more responsive to muscular loading (Moss and Young, 1960).

Most of the descriptions of modern human cranial robusticity come from clinical studies focused, for example, on quantifying mean CVT for surgical purposes. Published measures of adult cranial vault thickness range from 1.96 mm to 10.6 mm depending on

* Corresponding author.
E-mail address: lynn.copes@quinnipiac.edu (L.E. Copes).
[1] Current address: Frank H. Netter MD School of Medicine, Quinnipiac University, 275 Mt. Carmel Ave, NH-MED, Hamden, CT 06518, USA.

http://dx.doi.org/10.1016/j.jhevol.2015.08.008
0047-2484/

location on the vault (Adeloye et al., 1975; Brown, 1994; Hwang et al., 1997, 1999; Lynnerup, 2001; Jung et al., 2003; Moreira-Gonzalez et al., 2006). Allograft cranial-bone transplants using cadaver bone have become more common and have spurred increased research on the variation in CVT across the vault. For example, thickness purportedly increases from anterior to posterior across the parietal bone (Moreira-Gonzalez et al., 2006). Many investigators pick specific osteometric landmarks to measure, and most agree that *glabella* is the thickest point on the vault, followed by *vertex*, *opisthion*, and finally *euryon* (Anderson, 1882; Getz, 1960; Adeloye et al., 1975; Hwang et al., 1997, 1999; Friedland and Michel, 2006).

In several recent publications, variation in CVT across the vault (and even across single vault bones) has been assessed using mesh, grid, or semi-landmarks. These papers have found that single-landmark measurements do not capture the true variation of vault thickness (Balzeau, 2013; Marsh, 2013; Anzelmo et al., 2015).

Other work has addressed the question of the ontogeny of CVT in modern *Homo sapiens*, and reported that thickness increases in early life in step with increases in endocranial volume (Anzelmo et al., 2015) until the age of 20 and thereafter remains unchanged through adulthood (Lynnerup, 2001). A lack of an intraspecific scaling relationship between CVT and cranial capacity is not surprising, given frequent weakening of allometric relationships with decreasing taxonomic level (i.e., from order to species) (Copes and Schwartz, 2010).

A few workers have investigated the thickness of the diploë, either relative to total CVT or to age in modern humans. Lynnerup et al (2005) found a significant correlation between diploë thickness and total CVT in an autopsy sample of 64 modern humans, but failed to find significant associations between diploë thickness and age, height, or weight. Diploë thickness was measured on x-rays of trephined biopsies taken at four locations on dried skulls. Hatipolgu et al (2008) measured diploë thickness at seven landmarks on MR scans of 107 live adult subjects and reported significant linear correlations between age and diploë thickness at each landmark.

Variation in CVT among non-human primates has, to the best of our knowledge, been thoroughly investigated in only one study (Gauld, 1996). The goal of Gauld's study was to determine 1) if primate species are characterized by consistent patterns of interspecific variation in cranial thickness; 2) whether patterns of thickness in hominin species are concordant with those of other primates; or 3) whether deviations from typical patterns of cranial thickness occur with predictable regularity. Gauld chose to compare CVT with body mass. One of the most important aspects of an organism's biology is its body mass, which is highly correlated with certain key adaptations, including diet, locomotion, energetics, ecology, life history, morphology, and physiology. Body mass is thus one of the most commonly used metrics for exploring morphological allometric relationships.

Gauld (1992) found statistically significant relationships between CVT and body mass across her anthropoid sample (r values ranging from 0.94 to 0.97). She analyzed the relationships between body mass and CVT at different landmarks separately (rather than averaging all CVT measures), and in extant anthropoids the relationships were mostly positively allometric (slopes ranging from 0.40 to 0.53, where the slope for isometry is 0.33). Gauld did not test the relationship between vault or brain size and CVT, nor was she able to examine each bone layer individually. Her sample also did not include strepsirrhines.

When Gauld (1992) included *Australopithecus africanus*, "archaic" *H. sapiens*, and various regional groups of *H. erectus* in the regressions, slopes dramatically increased compared to the extant anthropoid analyses (0.45–2.63). Gauld's body masses of fossil hominins came from McHenry (1992) and Rightmire (1986), both of whom used postcranial size regressions to arrive at their estimates. While such analyses are ubiquitous in paleoanthropology, the use of cranial features such as cranial capacity or orbit size to estimate body mass have been argued to be both more practical (given the relative dearth of associated cranial and postcranial remains in the hominin fossil record) and as accurate as estimates relying on postcranial element scaling (Aiello and Wood, 1994; Kappelman, 1996; Plavcan, 2003).

Antón et al. (2007) explored the relationship between CVT at multiple landmarks and cranial capacity in fossil hominins. They reported a significant association within *H. erectus* between cranial capacity and bone thickness at *lambda* ($r^2 = 0.357$, slope = 0.862), thickness at the external occipital protuberance ($r^2 = 0.280$, slope = 0.930), and thickness at *asterion* ($r^2 = 0.509$, slope = 1.61). They reported no significant relationship between cranial capacity and thickness at midfrontal, *bregma*, or the parietal eminence.

Balzeau (2006, 2013) is one of the few workers to examine diploë thickness in fossil hominins. In 2006, he measured diploë and total CVT along the mid-sagittal plane from CT scans of four Ngandong and Sambungmacan fossils of *H. erectus* and compared them to measures taken on 12 modern *H. sapiens*. He produced a map of outer table, diploë, and inner table thickness along the mid-sagittal plane from *glabella* to opisthocranion, and was able to determine that whereas diploë constituted the majority of frontal bone thickness in most of the specimens he examined, all three layers contributed approximately equally to occipital thickness. Diploë thickness in the parietal region was not measurable, due to the presence of the sagittal suture. In his 2013 paper, Balzeau used a similar protocol to measure total CVT and quantify sagittal keeling in 120 specimens of recent and archaic *H. sapiens* and extant *Pan paniscus*, but he did not measure the thickness of each table separately.

Given previous suggestions regarding CVT in *H. erectus*, we here test two hypotheses:

1) Relative CVT is uniquely high in African and Asian *H. erectus* compared to other extant human and non-human primates; and
2) The vault composition of African and Asian *H. erectus* (quantified as the ratio of diploë to total thickness) is unique among primates.

Data collected for this endeavor allow for a previously impossible in-depth exploration of variation in CVT in the fossil record and across extant primates. These data will also be useful to test mechanistic hypotheses for increased CVT in the future.

2. Materials and methods

2.1. Non-human primate sample

A total of 452 non-human primate skulls housed at the Museum of Comparative Zoology and the Peabody Museum of Anthropology at Harvard University were microCT (μCT) scanned at Harvard's Center for Nanoscale Systems (CNS). From this sample, 255 female and 111 male adults were included in these analyses. Adulthood was determined by full eruption of the permanent third molars and canines. Any specimen with signs of bony pathology that might have impacted vault or facial growth was excluded. Specimens listed as captive were also not included. Specimens included in the final analyses came from 53 species representing all major families in the order Primates. The only major groups not included are *Phaner*, *Mirza*, *Allocebus*, and *Cheirogaleus* of the Cheirogaleiidae, *Lepilemur* of the Lepilemuridae, or any genus of Daubentoniidae or Tarsiidae. A summary of the sample size by sex per species is listed in Table 1.

Table 1
Non-human primate species included in this study and sample sizes by sex.

Suborder	(Sub)Family	Species	*n* adults (F, M)
Catarrhini	Cercopithecinae	*Cercocebus torquatus*	8 (1, 7)
		Cercopithecus mitis	10 (10, 0)
		Erythrocebus patas	4 (1, 3)
		Lophocebus albigena	7 (2, 5)
		Macaca fascicularis	8 (7, 1)
		Macaca fuscata	2 (0, 2)
		Macaca mulatta	3 (1, 2)
		Macaca sylvanus	2 (0, 2)
		Mandrillus leucophaeus	4 (0, 4)
		Mandrillus sphinx	2 (1, 1)
		Miopithecus talapoin	6 (3, 3)
		Papio anubis	9 (3, 6)
		Theropithecus gelada	1 (0, 1)
	Colobinae	*Colobus polykomos*	10 (9, 1)
		Nasalis larvatus	10 (10, 0)
		Piliocolobus badius	10 (5, 5)
		Presbytis hosei	5 (4, 1)
		Presbytis rubicunda	9 (5, 4)
		Trachypithecus cristatus	18 (18, 0)
	Hominidae	*Gorilla gorilla*	8 (8, 0)
		Hylobates lar	16 (16, 0)
		Pan paniscus	3 (2, 1)
		Pan troglodytes	13 (13, 0)
		Pongo pygmaeus	3 (3, 0)
		Symphalangus syndactylus	2 (2, 0)
Platyrrhini	Aotidae	*Aotus trivirgatus*	10 (8, 2)
	Atelidae	*Alouatta caraya*	4 (1, 3)
		Alouatta palliata	10 (10, 0)
		Ateles geoffroyi	18 (18, 0)
	Callitrichidae	*Callithrix argentata*	8 (4, 4)
		Callithrix humeralifer	4 (2, 2)
		Callithrix jacchus	2 (2, 0)
		Saguinus midas	10 (6, 4)
	Cebidae	*Cebus apella*	15 (8, 7)
		Cebus capucinus	10 (10, 0)
		Saimiri oerstedii	5 (1, 4)
		Saimiri sciureus	5 (2, 3)
	Pitheciidae	*Cacajao rubicundus*	2 (2, 0)
		Callicebus moloch	11 (0, 11)
		Chiropotes satanas	2 (2, 0)
		Pithecia monachus	4 (2, 2)
		Pithecia pithecia	3 (0, 3)
Strepsirrhini	Galagidae	*Galago alleni*	3 (2, 1)
		Galago senegalensis	12 (4, 8)
	Indriidae	*Avahi laniger*	5 (5, 0)
		Propithecus diadema	4 (2, 2)
		Propithecus verreauxi	5 (3, 2)
	Lemuridae	*Eulemur fulvus*	10 (10, 0)
		Hapalemur griseus	8 (7, 1)
		Lemur catta	5 (5, 0)
		Varecia variegata	6 (3, 3)
	Lorisidae	*Nycticebus coucang*	6 (3, 3)
		Perodicticus potto	10 (10, 0)
		Total:	371 (257, 114)

The scanner at CNS is a X-Tek HMXST225 μCT scanner with an open source X-ray tube with a maximum resolution of 3–5 μm. The X-ray detector panel was a Perkin Elmer 1621, which provides a 2000 × 2000 pixel and 16 inch × 16 inch (40.64 cm × 40.64 cm) field of view with a 7.5 frames per second readout and a physical pixel size of 200 microns. The energy settings for each scan ranged between 70 and 90 kV and 90–125 μA, depending on the size of the specimen. The strepsirrhine and smaller catarrhine specimens were scanned without filters, while *Pan, Pongo,* and *Gorilla* specimens were scanned with a tungsten filament filter to minimize beam hardening.

Each skull was placed in a foam holder that was then positioned inside the scanner on a rotating platform. The Styrofoam held the skull in place while still allowing the X-rays to fully penetrate the specimen without leaving visual artifacts. All crania in this study were scanned at parameters optimum for the highest possible resolution within the time available to capture all samples. All crania were scanned using 1000–1500 projections, scan time per specimen ranged from 18 to 60 min, and resolution ranged from 18 μm for smaller specimens (e.g., *Callithrix*) to 125 μm for the largest (e.g., *Pongo*) (See Supplementary Online Material [SOM] Table 1 for all sample scanning parameters.) Cranial capacity was obtained from each individual using sesame seeds. All non-human primate scans are freely available for download through the MCZ mammalogy database or Morphosource.org, hosted by Duke University.

2.2. Human sample

Five hundred and seventy modern human skulls were CT-scanned in the anthropology department at the National Museum of Natural History, Smithsonian Institution, Washington, DC (SOM Table 2; summarized in Table 2). The entire skull of each individual (or just the cranium if an associated mandible was not available) was CT scanned using a Siemens Somatom spiral scanner (70 mA, 110 kV, slice width 1.0 mm, reconstruction 0.5 mm). This represented the highest resolution possible on the scanner at the time of scanning.

The humans included in this sample came from archaeological sites in Alaska, Greenland, Oceania, and from the Terry Collection, a cadaver-based skeletal collection of individuals living in the United States in the late 19th and early 20th century. Cranial capacity was obtained from each individual using sesame seeds. All human skull CT scans are available upon request.

2.3. Cranial vault thickness algorithm

CVT in extant human and non-human primates was measured from CT scans automatically by an algorithm written expressly for this project. Each scan was imported to the Scanco μCT 40 at Stony Brook University, converted from DICOM to .isq format, and anonymized so that the sex, species, and/or geographic locality (in the case of the modern humans) was unknown to the evaluator. The algorithm, written by Svetlana Lublinsky, is a modified version of an automated algorithm written to detect the trabecular-cortical bone interface in long bones. Details about the long-bone algorithm, along with code, can be found in Lublinsky et al. (2007).

The algorithm automatically finds the boundary between bone and air using the voxel brightness, which is assigned based on attenuation, or the amount of X-ray energy the material absorbs. The Scanco μCT system converts individual attenuation measurements into Hounsfield units by comparing specimen absorption

Table 2
Human populations included in this study and sample sizes by location and sex.

Locality		*n* adults (F, M)
Oceania	Australia	21 (12, 9)
	Indonesia	14 (6, 8)
	New Zealand	20 (12, 8)
	Papua New Guinea	31 (17, 14)
	Philippines	10 (6, 4)
Eskimo	Greenland	61 (35, 26)
	Point Hope, Alaska: Ipiutak	37 (18, 19)
	Point Hope, Alaska: Tigara	207 (112, 95)
	Point Hope, Alaska: unspecified	73 (35, 38)
Modern	Terry Collection	96 (29, 67)
Total:		570 (282, 288)

values to a standard calibration phantom provided by the manufacturer (http://www.scanco.ch/index.php?id=faq_general#c926). The algorithm then detects the bone – air boundary using an automated thresholding paradigm (Lublinsky et al., 2007).

After detecting the bone – air boundary, the algorithm selects three cylindrical volumes of interest (VOIs) on the frontal, and right and left parietal bones. To place the VOIs, the algorithm encloses the skull in a rectangle, which it bisects coronally to create a "frontal" box, in which the frontal VOI is centered. The posterior box is then bisected sagittally to create two "parietal" boxes, in which the parietal VOIs are centered.

Each VOI was 60 pixels in diameter, and since smaller skulls were scanned at higher resolution than larger skulls, the VOI was scaled to the size of the skull, and captured an approximately equal percentage of the bone on galagos as on gorillas. The 60-pixel VOIs did capture a slightly smaller overall percentage of human skulls than comparably-sized ape skulls, because the humans were scanned at a lower resolution. However, given that human cranial capacity is approximately three times that of extant great apes, and the resolution of human CT scans was approximately three times lower than that of the great ape scans, we believe the volumes analyzed are comparable across the entire sample. The VOIs were positioned to avoid any sutures (Fig. 1).

The algorithm measures the thickness of the total bone at each pixel within the VOI and then masks the trabecular bone (diploë) and calculates its thickness at each pixel. The cortical – trabecular boundaries were calculated using an automated thresholding paradigm written into the algorithm. Thickness was calculated using a sphere-fitting method, by which the diameters of the largest possible spheres that can be fitted through each voxel (remaining completely contained within the object or layer) are calculated and averaged across the VOI (Bouxsein et al., 2010).

The results reported by the algorithm included mean, median, and maximum total thickness of each of the three VOIs, as well as mean thickness of the diploë layer of each. We calculated mean cortical thickness by subtracting mean diploë thickness from mean total thickness. We are confident that the resolution of the scans was adequate to accurately measure both total CVT and diploë thickness, as the minimum ratio of voxel size to thickness of structures measured is 2:1, the ideal is greater than 5:1 (Bouxsein et al., 2010), and across our sample, the ratio between voxel size and diploë thickness (the smallest measurement of interest) averaged 7.4 (range 3.4–16.7).

A final variable was calculated from the data provided by the algorithm by dividing reported average diploë thickness of the VOI by that VOI's reported thickness of the entire vault.

Variables from the right and left parietal VOIs were averaged, resulting in measurements for a single "parietal" unit. While several recent works have commented on the variation in CVT across the vault (Balzeau, 2013; Marsh, 2013; Anzelmo et al., 2015), we are unaware of any evidence suggesting that the right and left parietals are asymmetrical in terms of thickness. To simplify the resulting analyses, we chose to average the parietal measurements.

2.4. Fossil hominin sample

The majority of the data for fossil hominins were gathered from previously published accounts, including Gauld (1996), Lieberman (1996), and Kimbel et al. (2004). The published data used, along with original measurements collected, are listed in SOM Table 3.

Most measurements provided in the published literature were taken at landmarks––*bregma* and *lambda* are the most commonly measured sites. The parietal eminence is also frequently measured, but as this is not at a sutural intersection it is possible that different researchers chose different spots for the point measurement on the same specimen. Gauld (1996) included several mid-bone sites (mid-frontal and several different mid-parietal sites), but still limited her thickness measures to a single point. All published figures are measurements of whole bone thickness (sources for every literature-derived measurement are listed in SOM Table 3). Measuring total thickness at landmarks likely lowers inter- and intraobserver error, although several published thickness measures purportedly taken at the same point on the same fossil differ by more than a millimeter from one researcher to another. Because original fossil material was generally unavailable for additional measurement (although see below for exceptions), every published measure found in the literature was used to calculate species means for the frontal and parietal bones. Many landmarks fall on the boundary of two bones, so the decision was made to use measurements at *bregma* in calculations of frontal bone thickness and measurements at *lambda* were excluded because they were

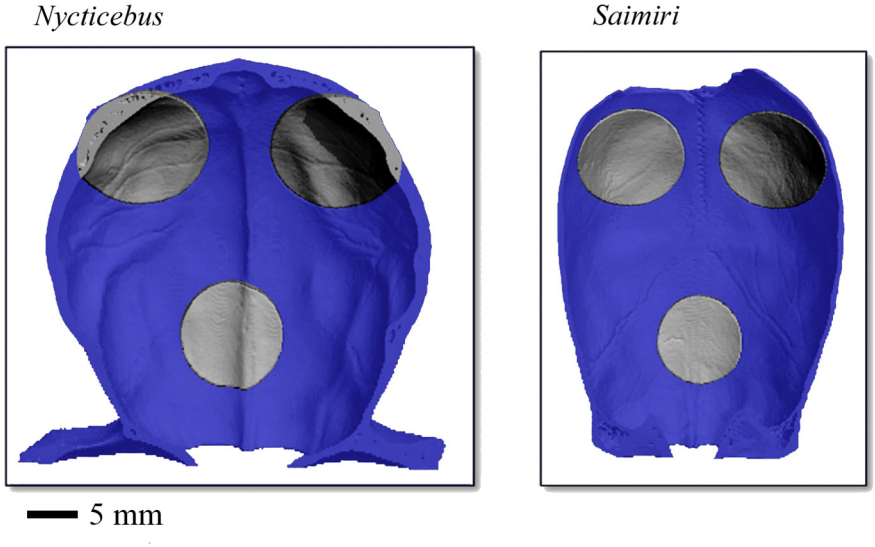

Figure 1. Examples of the placement of circular ROIs on the frontal and both parietal bones of primate CT scans to measure cranial vault thickness.

determined to be indicative of occipital bone thickness. Also, in the literature not all metrics were recorded with note made of taphonomic factors than can alter the thickness of cranial bone (erosion, expansion cracking, etc.), yet this is almost certainly the case with a number of specimens included in these analyses.

Original fossil material was measured at the National Museum of Ethiopia (NME, Addis Ababa) and National Museums of Kenya (NMK, Nairobi). Rather than taking single total thickness measurements at landmarks on mostly intact skulls, we focused on multiple measures of thickness taken along the broken edges of vault fragments.

Cranial vault fragments attributed to *Australopithecus afarensis, Paranthropus boisei, Homo habilis, Homo rudolfensis*, and *H. erectus* (including *Homo ergaster* of some authors) were photographed at NME and NMK. Fragments were photographed only if they did not display obvious erosion or weathering to the inner or outer table. Some fragments were eroded in some areas and not others; photographs were then taken only of the unweathered portions. Wear to the exposed broken edge of the vault (for example, a rounded lip) was not cause for immediate exclusion of the specimen if the (presumed) unworn thickness of the bone could be detected close enough to the edge to capture in focus. Intact crania were photographed occasionally, but only when natural breaks in the vault was large enough to visualize the broken edge fully.

Fragments were photographed using a tripod-mounted Nikon D3000 10.2 MP DSLR camera with a macro lens. Bone fragments were positioned in a beanbag so that their broken edges were parallel to the camera lens. To minimize distortion of the object, the camera was kept as far from the bone as possible, and the zoom function on the camera used to maximize the size of the bone in the image. A bulls-eye scale was placed in the frame at the level of the bone surface, and the position of the bone surface, scale, and camera checked with a spirit level. The majority of the fragments were photographed using aperture f/16 and shutter speed 1/3 s. All photographs were taken using a remote shutter release to minimize camera vibration.

Photographs were measured using ImageJ (http://rsb.info.nih.gov/ij/). The scale in the photograph was measured and ImageJ's scale set for the appropriate distance (1 cm). Bone thickness was then measured at multiple points along the edge of the fragment in focus in the picture. Measurements were spaced approximately 0.5 cm apart, so a 5 cm section of vault would be measured at 10 separate locations. The measurements were taken perpendicular to the external table. Where possible, the three layers were measured separately, but in many cases the internal boundaries were indiscernible. Figure 2 shows two fragments, one with clear boundaries between tables and one without. The measurements taken from each photograph were averaged, but the measurements taken from different photographs of each specimen are listed separately in the results.

2.4.1. Landmark vs. off-landmark thickness Many of the data on fossil hominin CVT used in this analysis came from published measurements. There are benefits and drawbacks to these published figures. The benefits are an increased sample size for fossils we were unable to measure ourselves. However, previous studies of cranial vault thickness (e.g., Nawrocki, 1991; Gauld, 1996; Lieberman, 1996) and nearly all reports of CVT taken on fossil hominins (e.g., Todd, 1924; Weidenreich, 1943; Roche, 1953; Singer, 1954; Tobias, 1967; Jacob, 1973; Day et al., 1976, 1980; Asfaw, 1983; Magori and Day, 1983; Wood, 1984; Clarke, 1985; Bräuer and Leakey, 1986; Kennedy, 1991; Walker and Leakey, 1993; Brown, 1994; Antón, 1999, 2004; Kimbel et al., 2004) have measured CVT at specific landmarks, usually *bregma* and the parietal eminence. We chose to measure CVT on cylindrical volumes of interest in the middle of the frontal and parietal bones for several reasons: 1) some cranial superstructures are located along sutures, inflating the thickness measures taken there compared to the average thickness of the bone; 2) the three tables (inner, outer, diploë) are most distinct away from the sutures; 3) calculating the average thickness of a 2–5 cm diameter volume of interest is more likely to capture the average thickness of the vault bones than is measuring a single point, where the thickness likely overestimates that of the average vault bone.

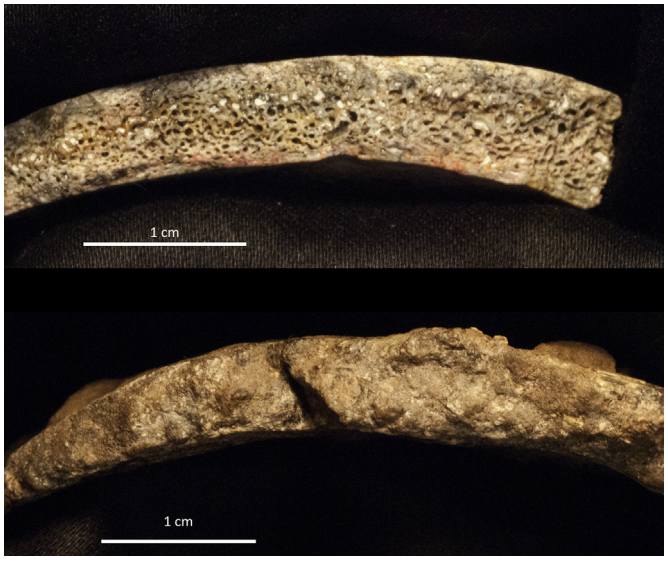

Figure 2. Photographs of KNM-ER 1800 (top) and KNM-ER 1590 (bottom). Diploë thickness could be measured in KNM-ER 1800, but not in this fragment of KNM-ER 1590.

A separate study of CVT on and off the sutures would be interesting for several reasons. Behrents et al. (1978) found increased masticatory-induced strain on sutural, as opposed to off-sutural, bone in two juvenile macaques. Byron et al. (2004) demonstrated increased osteogenesis at the sutures with increased loading in a mouse model with enlarged temporalis muscle mass and strength. Peptan et al. (2008) found increased osteoblast densities along the premaxillomaxillary and nasofrontal sutures in rabbits subjected to cyclic tensile or compressive forces applied to the maxilla. On the other hand, Rawlinson et al (1995) dynamically loaded ulnae and calvariae in rats and found that calvarial osteocytes and osteoblasts failed to respond (via increased glucose 6-phosphate dehydrogenase activity or prostaglandin release) to cyclic loading, while ulnar cells showed increased excitation. It is possible that sutural bone is more responsive to loading than non-sutural vault bone. Off-sutural CVT is certainly worthy of investigation in the future, although it was beyond the scope of the current project.,

2.4.2. Comparing measurements taken from CT scans and photographs One of the most obvious drawbacks to a study comparing fossil and extant skeletal specimens is that the methods used to garner measurements are not always identical. In this case, intact human and non-human primate skulls were CT scanned and measured using an algorithm while fossil fragments were photographed and measured via computer. In an ideal world, CT scans of fossil material would be widely available and of sufficient quality to use the same measuring algorithm. However, while fossil material is increasingly being scanned, those scans are not yet widely available, and the scans that are available are often difficult to read due to the density of the bone turned to rock. The relative thickness of cortical and diploë layers was not measureable in CT scans of any fossil material we were able to access. Thus, in order to investigate the second hypothesis and

measure off-landmark thickness, we chose to photograph and measure the fossil material instead.

To test the comparability of thickness data acquired via CT algorithm to that measured linearly from photographs, we randomly selected three non-human primate and two human CT scans, chose 12 slices (in either a coronal or sagittal plane) that included a portion of a frontal or parietal VOI, and measured the total CVT and diploë thickness in ImageJ using the fossil hominin measurement protocol. Total thickness was overestimated by the ImageJ protocol relative to the algorithm by 1–4%, and diploë thickness was overestimated by 3–10%. Even 10% error in a measurement of a CT scan taken at the resolutions these skulls were translates to <500 μm, a difference that would have been difficult to detect with calipers. We are confident that the algorithm and ImageJ measurements are similar enough to allow comparison of data collected with each modality.

2.5. Residual analysis

To determine if *H. erectus* CVT values are uniquely high among extinct hominins or all primates, a residual analysis was undertaken. First, sex-specific species mean CVT of each bone was plotted against species mean cranial capacity (following Antón et al., 2007) for the entire sample. The relationship between the two variables in the extant non-human primate sample was found using Reduced Major Axis (RMA) regression. RMA was performed in this case based on the recommendation of Smith (2009). The RMA slope is calculated assuming symmetric error in both X and Y variables, and is less prone to overestimate the extent to which residuals are positive in the large-bodied hominins, which fall outside the range of extant non-human primate data (Warton et al., 2006). Residual analysis was used rather than a ratio test because we were interested in controlling for overall size, rather than examining the proportionality of the two measures (Smith, 2005).

Once RMA slopes were established for the species means, every individual's vertical deviation from the regression lines was calculated. Species mean residuals were then calculated and ranked. Differences in species means among species with the ten thickest residual values were determined using general linear-mixed model procedure allowing for heterogenous variance.

3. Results

3.1. Does Homo erectus have uniquely thick cranial vaults?

The residual analyses were performed using male and female human and non-human primates separately, although all fossil specimens were included in both analyses. Frontal and parietal thicknesses were tested separately. Thus, four different residual analyses were performed in total. Results of female RMA analyses are shown here, with results of the other analyses discussed here, but data presented in the accompanying SOM.

To calculate residual CVT, total frontal or parietal CVT was plotted against cranial capacity, as illustrated in Figure 3. The RMA slope was calculated using extant non-human primate species means. In the case of female NHP frontal thickness, the RMA slope was 0.47 ± 0.05, which is significantly positively allometric with respect to an isometric slope of 0.33. Using the RMA slope derived from species mean values, residuals for each individual specimen were calculated to provide a species mean residual with a measure of variation. Fossil hominin and extant female species mean cranial capacity and total frontal thickness, along with predicted total frontal thickness using RMA regression, RMA residuals, and the rank of those residuals, are shown in Table 3. A clearer visualization of the 10 species with the highest RMA residuals for frontal thickness is shown in Table 4, and a boxplot of the residuals for each of the species listed in Table 4 is shown in Figure 4. African *H. erectus* is ranked second, and Asian *H. erectus* is ranked fourth, and African *H. erectus* frontal residual thickness is not significantly greater than Asian *H. erectus* ($p = 0.07$). Four extant non-human primates, *Nycticebus coucang*, *Alouatta caraya*, *Perodicticus potto*, and *Lophocebus albigena* are ranked first, fifth, seventh, and ninth respectively. The species with the thickest frontal bone for its brain size is *N. coucang*, but its residual value for frontal thickness is not significantly higher than the other ten species with the next highest residuals. Finally, female Holocene *H. sapiens* ranks 38th in frontal residual derived from female non-human primate RMA regression, which is significantly thinner than both African ($p < 0.001$) and Asian *H. erectus* ($p < 0.001$) as well as the other eight species with the thickest relative frontal bones (p values range from <0.001 to 0.01).

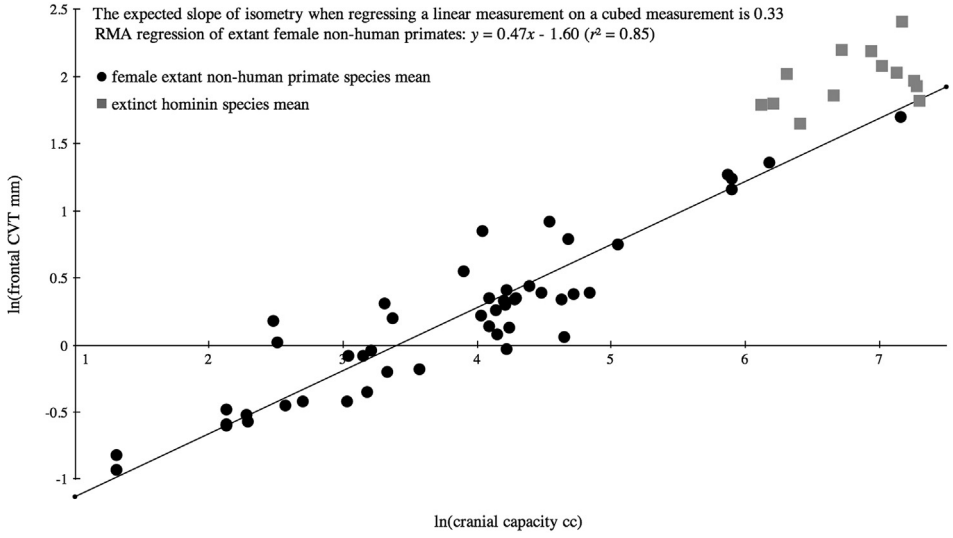

Figure 3. Scatterplot of total frontal thickness versus cranial capacity. Extant female non-human primate species means are represented by black circles; hominin species means are represented by gray squares. The RMA slope was calculated using the extant non-human primates. The slope (0.47) is positively allometric relative to an expected slope of isometry of 0.33.

Table 3
Mean cranial capacity and actual frontal thickness for each species; predicted thickness given RMA slope[a] calculated using species means of extant female non-human primates; RMA residuals and rank of those residuals relative to the other 56 species.

Species	n[b]	ln(cc)	ln(total frontal thickness) (mm)		RMA residual	RMA residual rank
			Actual (SD)	RMA prediction		
Australopithecus afarensis	2	6.31	2.01 (0.59)	1.37	0.64	3
Australopithecus africanus	10	6.14	1.82 (0.47)	1.29	0.53	6
Paranthropus boisei	7	6.20	1.79 (0.18)	1.31	0.48	8
Early *Homo*	10	6.53	1.79 (0.40)	1.47	0.32	13
African *Homo erectus*	8	6.72	2.22 (0.26)	1.56	0.66	2
Asian *Homo erectus*	29	6.94	2.22 (0.74)	1.66	0.56	4
Homo heidelbergensis	14	7.13	2.14 (0.59)	1.75	0.39	10
Homo neanderthalensis	13	7.30	1.89 (0.47)	1.83	0.06	25
Pleistocene *Homo sapiens*	17	7.34	2.01 (0.74)	1.85	0.16	17
Holocene *Homo sapiens* (females only)	282	7.16	1.72 (0.26)	1.77	−0.05	38
Alouatta caraya	1	4.04	0.85 (−)	0.30	0.55	5
Alouatta palliata	10	3.91	0.59 (−0.64)	0.24	0.35	12
Aotus trivirgatus	8	2.70	−0.40 (−2.44)	−0.33	−0.07	40
Ateles geoffroyi	18	4.63	0.36 (−1.40)	0.58	−0.22	47
Avahi laniger	5	2.28	−0.53 (−3.21)	−0.53	0.00	32
Cacajao melanocephalus	2	4.20	0.36 (−0.80)	0.37	−0.02	34
Callithrix argentata	4	2.13	−0.58 (−2.94)	−0.60	0.02	28
Callithrix humeralifera	2	2.13	−0.46 (−2.29)	−0.60	0.14	18
Callithrix jacchus	2	2.13	−0.60 (−2.70)	−0.60	0.00	31
Cebus apella	8	4.16	0.10 (−1.65)	0.35	−0.26	54
Cebus capucinus	10	4.22	−0.03 (−2.12)	0.38	−0.41	56
Cercocebus torquatus	1	4.62	0.34 (−)	0.57	−0.23	48
Cercopithecus mitis	10	4.15	0.26 (−1.86)	0.35	−0.09	41
Chiropotes satanas	2	4.03	0.22 (−1.91)	0.29	−0.07	39
Colobus polykomos	9	4.28	0.36 (−1.24)	0.41	−0.05	37
Erythrocebus patas	1	4.48	0.38 (−)	0.50	−0.12	44
Eulemur fulvus	10	3.15	−0.06 (−1.94)	−0.12	0.06	27
Galago alleni	2	1.31	−0.82 (−3.71)	−0.99	0.16	16
Galago senegalensis	4	1.31	−0.92 (−3.46)	−0.99	0.07	24
Gorilla gorilla	8	6.19	1.40 (0.18)	1.31	0.09	21
Hapalemur griseus	7	2.58	−0.43 (−2.25)	−0.39	−0.04	36
Hylobates lar	16	4.66	0.08 (−1.63)	0.59	−0.51	57
Lemur catta	5	3.04	−0.06 (−1.66)	−0.17	0.11	20
Lophocebus albigena	2	4.54	0.95 (0.02)	0.54	0.42	9
Macaca fascicularis	6	4.10	0.38 (−1.47)	0.33	0.06	26
Macaca mulatta	1	4.72	0.38 (−)	0.62	−0.24	51
Mandrillus sphinx	1	4.68	0.79 (−)	0.60	0.19	15
Miopithecus talapoin	3	3.57	−0.17 (−2.66)	0.08	−0.25	53
Nasalis larvatus	10	4.39	0.45 (−1.36)	0.46	−0.01	33
Nycticebus coucang	3	2.48	0.29 (−1.48)	−0.44	0.72	1
Pan paniscus	2	5.90	1.18 (0)	1.17	0.01	29
Pan troglodytes	13	5.90	1.25 (−0.42)	1.17	0.08	22
Papio anubis	3	5.05	0.75 (−2.69)	0.78	−0.03	35
Perodicticus potto	5	2.48	0.10 (−1.63)	−0.43	0.53	7
Piliocolobus badius	5	4.27	0.41 (−1.76)	0.40	0.01	30
Pithecia monachus	2	3.35	−0.14 (−2.64)	−0.03	−0.11	43
Pongo pygmaeus	3	5.87	1.29 (0)	1.16	0.13	19
Presbytis hosei	4	4.24	0.14 (−1.47)	0.39	−0.25	52
Presbytis rubicunda	5	4.23	0.25 (−1.68)	0.39	−0.14	45
Propithecus diadema	2	3.31	0.32 (−1.15)	−0.04	0.36	11
Propithecus verreauxi	4	3.18	−0.03 (−2.44)	−0.11	0.08	23
Saguinus midas	4	2.29	−0.62 (−2.01)	−0.52	−0.09	42
Saimiri oerstedii	1	3.18	−0.34 (−)	−0.11	−0.24	50
Saimiri sciureus	2	3.02	−0.42 (−2.88)	−0.18	−0.24	49
Symphalangus syndactylus	2	4.84	0.39 (−1.95)	0.68	−0.29	55
Trachypithecus cristatus	18	4.09	0.15 (−2.18)	0.32	−0.17	46
Varecia variegata	2	3.30	0.22 (−2.09)	−0.05	0.27	14

[a] RMA: ln(total frontal thickness) = 0.47*ln(CC) − 1.60.
[b] *n* indicates the number of individuals included in the calculation of species mean values – for the fossil species, more than one measurement may have been included per individual.

The pattern of relative parietal bone thickness calculated with RMA regression using the female extant primate sample is broadly similar to that of the frontal bone analysis. The entire list of all extant species with female specimens and all of the fossil specimens with cranial capacity, actual parietal thickness, predicted thickness using RMA regression, residuals, and residual rankings, is given in SOM Table 4; the species with the top ten relative parietal bone thicknesses are listed in Table 5. In the case of the RMA regression analysis of parietal bone thickness, five extant non-human primates are among those with the thickest bones: *N. coucang*, *P. potto*, *Propithecus diadema*, *Pongo pygmaeus*, and *L. albigena*, which are ranked first, second, seventh, ninth, and tenth respectively. Asian *H. erectus* is ranked third, while African *H. erectus* is ranked eighth; the difference between these two parietal residual thickness values is significant ($p < 0.001$). The female modern humans' sample ranks 43rd in parietal thickness, and all

Table 4
Ten species (females only) with the thickest relative frontal bones using RMA regression.[a]

Species	n[b]	ln(cc)	ln(total frontal thickness) (mm)		RMA residual	RMA residual rank
			Actual (SD)	RMA prediction		
Nycticebus coucang	3	2.48	0.29 (−1.48)	−0.44	0.72	1
African *Homo erectus*	8	6.72	2.22 (0.26)	1.56	0.66	2
Australopithecus afarensis	2	6.31	2.01 (0.59)	1.37	0.64	3
Asian *Homo erectus*	29	6.94	2.22 (0.74)	1.66	0.56	4
Alouatta caraya	1	4.04	0.85 (−)	0.30	0.55	5
Australopithecus africanus	10	6.14	1.82 (0.47)	1.29	0.53	6
Perodicticus potto	5	2.48	0.10 (−1.63)	−0.43	0.53	7
Paranthropus boisei	7	6.20	1.79 (0.18)	1.31	0.48	8
Lophocebus albigena	2	4.54	0.95 (0.02)	0.54	0.42	9
Homo heidelbergensis	14	7.13	2.14 (0.59)	1.75	0.39	10

Notes on differences in residuals:
N. coucang is not significantly thicker than other top ten species.
N. coucang is significantly thicker than Holocene *Homo sapiens* females (ranked 38; $p = 0.025$).
Asian & African *H. erectus* are both significantly thicker than Holocene *H. sapiens* (both $p < 0.001$).
African *H. erectus* is significantly thicker than Asian *H. erectus* ($p = 0.032$).
[a] RMA: ln(total frontal thickness) = 0.47*ln(CC) − 1.60.
[b] n indicates the number of individuals included in the calculation of species mean values – for the fossil species, more than one measurement may have been included per individual.

species with the ten thickest parietal residual values have significantly thicker bones than modern human females (p values range from <0.001 to 0.046).

Comparing the fossils to male non-human primates changes the results somewhat, because not all non-human primate species included in the analysis were represented by both male and female individuals; thus, the species included in the analysis differed. The overall patterns, however, were the same. Using male non-human primates and RMA regression, African and Asian *H. erectus* frontal bones were not uniquely thick (all data in SOM Table 5; extremes in Table 6). African *H. erectus* ranks third, and Asian *H. erectus* ranks sixth; African *H. erectus* frontal bones are not significantly thicker than Asian *H. erectus* ($p = 0.058$). *A. caraya, N. coucang, Galago alleni, P. diadema,* and *P. potto* all make the top ten list, at first, second, seventh, ninth, and tenth respectively. None of the species in the top ten differed significantly from *A. caraya*. Male humans rank 38th among primates in relative frontal thickness, and all species with the ten thickest frontal residual values have significantly thicker bones than modern human males (p values all <0.001).

Parietal bone residual thickness calculated using male non-human primates follows the same general pattern of the other analyses (all data in SOM Table 6; extremes in Table 7). Asian *H. erectus* ranks fourth, while African *H. erectus* ranks tenth; the Asian mean is significantly greater than the African mean ($p < 0.001$). Extant primates with thick parietal bones are *A. caraya* (ranked first), *P. potto* (second), *N. coucang* (third), *G. alleni* (fifth), and *Mandrillus sphinx* (ninth). *A. caraya* residual parietal thickness values are not significantly thicker than the other top seven ranked species. Male humans rank 39th in parietal thickness, and all species with the ten thickest parietal residual values have significantly thicker bones than modern human males (p values all <0.001).

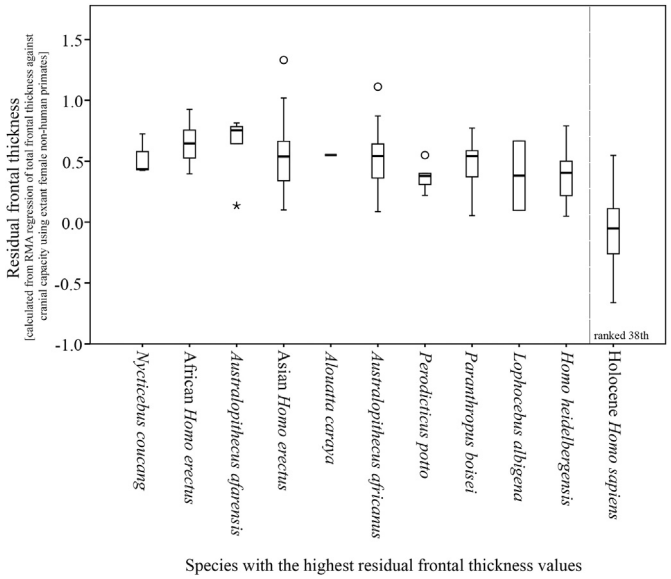

Figure 4. Boxplots of residuals of relative frontal thickness. Calculated by determining individual variation from a regression of total frontal thickness on cranial capacity calculated using species mean values of female non-human primates. The variation in species residual is shown for the species with the 10 highest species mean residual values. Holocene *Homo sapiens* is included on the far right for reference.

3.2. Are Homo erectus vaults built in the same way as other species with thick bones?

The question of vault-bone composition (i.e., the relative thickness of diploë and cortical bone) is complicated by the fact that diploë thickness is not available for most of the fossil specimens, including Asian *H. erectus*. Thus, we can only compare diploë ratio of a few fossil parietal bones to extant human and non-human primate parietal bones. Additionally, several non-human primate species are represented in our sample by female specimens only, limiting some potential comparisons.

The parietal residual thickness and diploë ratios (where known) of the species included in the study are listed in Table 8. The species are sorted by residual parietal thickness, so the species at the top are those with the thickest parietal bones relative to cranial capacity. Modern humans and fossil hominins, which are in bold, have diploë ratios above 0.48 (except *Paranthropus boisei*). The male non-human primates with the thickest relative parietal bones all have diploë ratios of less than 0.43, and female non-human primates with the thickest relative parietal bones have diploë ratios of less than 0.41. To examine the scaling of diploë ratio to total thickness, a scatterplot of female species means of logged parietal thickness and logged parietal diploë ratio is shown in Figure 5. There is no relationship among the extant non-human primates (RMA slope = −1.25; $r^2 = 0.18$), indicating that diploë ratio seems unrelated to total *raw* parietal thickness. However, we chose to

Table 5
Ten species (females only) with the thickest relative parietal bones using RMA regression.[a]

Species	n[b]	ln(cc)	ln(total parietal thickness)		RMA residual	RMA residual rank
			Actual	RMA prediction		
Nycticebus coucang	3	2.48	0.08 (−1.66)	−0.66	0.73	1
Perodicticus potto	5	2.48	0.02 (−1.56)	−0.65	0.67	2
Asian *Homo erectus*	33	6.95	2.32 (0.74)	1.73	0.59	3
Australopithecus africanus	13	6.21	1.81 (0.18)	1.34	0.47	4
Homo heidelbergensis	17	7.12	2.24 (0.83)	1.83	0.41	5
Paranthropus boisei	7	6.18	1.72 (0.59)	1.33	0.40	6
Propithecus diadema	2	3.31	0.11 (−1.24)	−0.21	0.32	7
African *Homo erectus*	15	6.72	1.92 (0.34)	1.61	0.31	8
Pongo pygmaeus	3	5.87	1.40 (0.23)	1.16	0.24	9
Lophocebus albigena	2	4.54	0.68 (−0.99)	0.45	0.23	10

Notes on differences in residuals:
N. coucang is not significantly thicker than other top ten species.
N. coucang is significantly thicker than Holocene *Homo sapiens* females (ranked 43; $p = 0.05$).
Asian & African *H. erectus* are both significantly thicker than Holocene *H. sapiens* (both $p < 0.001$).
Asian *H. erectus* is significantly thicker than African *H. erectus* ($p < 0.001$).
[a] RMA: ln(total parietal thickness) = 0.53*ln(CC) − 1.98.
[b] *n* indicates the number of individuals included in the calculation of species mean values – for the fossil species, more than one measurement may have been included per individual.

Table 6
Ten species (males only) with the thickest relative frontal bones using RMA regression.[a]

Species	n[b]	ln(cc)	ln(total frontal thickness)		RMA residual	RMA residual rank
			Actual	RMA prediction		
Alouatta caraya	3	4.00	1.09 (0.17)	0.34	0.75	1
Nycticebus coucang	3	2.48	0.10 (−1.61)	−0.42	0.53	2
African *Homo erectus*	8	6.72	2.22 (0.26)	1.70	0.52	3
Australopithecus afarensis	2	6.31	2.01 (0.59)	1.49	0.52	4
Australopithecus africanus	10	6.14	1.82 (0.47)	1.41	0.41	5
Asian *Homo erectus*	29	6.94	2.22 (0.74)	1.81	0.41	6
Galago alleni	1	1.31	−0.60 (−)	−1.01	0.41	7
Propithecus diadema	2	3.20	0.33 (−1.43)	−0.06	0.39	8
Paranthropus boisei	7	6.20	1.79 (0.18)	1.44	0.35	9
Perodicticus potto	5	2.55	−0.04 (−2.21)	−0.39	0.34	10

Notes on differences in residuals:
A. caraya is not significantly thicker than other top ten species.
A. caraya is not significantly thicker than Holocene *Homo sapiens* males (ranked 38; $p = 0.082$).
Asian & African *H. erectus* are both significantly thicker than Holocene *H. sapiens* (both $p < 0.001$).
African *H. erectus* is significantly thicker than Asian *H. erectus* ($p = 0.025$).
[a] RMA: ln(total frontal thickness) = 0.50*ln(CC) − 1.66.
[b] *n* indicates the number of individuals included in the calculation of species mean values – for the fossil species, more than one measurement may have been included per individual.

Table 7
Ten species (males only) with the thickest relative parietal bones using RMA regression.[a]

Species	n[b]	ln(cc)	ln(total parietal thickness)		RMA residual	RMA residual rank
			Actual	RMA prediction		
Alouatta caraya	3	3.995077	1.02 (−0.33)	0.24	0.78	1
Perodicticus potto	5	2.549445	0.00 (−2.21)	−0.56	0.56	2
Nycticebus coucang	3	2.476538	−0.07 (−1.31)	−0.60	0.53	3
Asian *Homo erectus*	33	6.95	2.32 (0.74)	1.86	0.46	4
Galago alleni	1	1.308333	−0.87 (−)	−1.24	0.37	5
Australopithecus africanus	13	6.21	1.81 (0.18)	1.46	0.35	6
Homo heidelbergensis	17	7.12	2.24 (0.83)	1.96	0.28	7
Paranthropus boisei	7	6.18	1.72 (0.59)	1.44	0.28	8
Mandrillus sphinx	1	5.247024	1.18 (−)	0.93	0.26	9
African *Homo erectus*	15	6.72	1.92 (0.34)	1.73	0.19	10

Notes on differences in residuals:
A. caraya is not significantly thicker than other top seven species.
A. caraya is significantly thicker than Holocene *Homo sapiens* males (ranked 39; $p = 0.02$).
Asian & African *H. erectus* both significantly thicker than Holocene *H. sapiens* (both $p < 0.001$).
Asian *H. erectus* significantly thicker than African *H. erectus* ($p < 0.001$).
[a] RMA: ln(total parietal thickness) = 0.55*ln(CC) − 1.96.
[b] *n* indicates the number of individuals included in the calculation of species mean values – for the fossil species, more than one measurement may have been included per individual.

Table 8
Mean parietal residual thickness and parietal diploë ratio for species included in the analysis, split by sex. Bolded values are human and hominin species.

Species (female specimens and fossils only)	*n*	Parietal residual	Parietal diploë ratio
Nycticebus coucang	3	0.73	0.32
Perodicticus potto	5	0.67	0.33
Asian *Homo erectus*	**33**	**0.59**	–
Australopithecus africanus	**13**	**0.47**	–
Homo heidelbergensis	**17**	**0.41**	–
Paranthropus boisei	**7**	**0.40**	**0.43**
Propithecus diadema	2	0.32	0.41
African *Homo erectus*	**15**	**0.31**	**0.52**
Pongo pygmaeus	3	0.24	0.39
Lophocebus albigena	2	0.23	0.32
Gorilla gorilla	8	0.22	0.25
Alouatta palliata	10	0.20	0.35
Alouatta caraya	1	0.19	0.37
Homo neanderthalensis	**35**	**0.18**	–
Callithrix argentata	4	0.17	0.46
Callithrix humeralifera	2	0.15	0.38
Papio anubis	3	0.15	0.31
Early *Homo*	**13**	**0.15**	**0.52**
Varecia variegata	2	0.14	0.51
Propithecus verreauxi	4	0.13	0.41
Mandrillus sphinx	1	0.13	0.37
Pan paniscus	2	0.13	0.21
Australopithecus afarensis	**8**	**0.12**	**0.50**
Pleistocene *Homo sapiens*	**31**	**0.11**	–
Galago alleni	2	0.11	0.39
Callithrix jacchus	2	0.11	0.47
Avahi laniger	5	0.11	0.46
Saguinus midas	4	0.08	0.46
Lemur catta	5	0.07	0.46
Eulemur fulvus	10	0.06	0.56
Pan troglodytes	13	0.05	0.22
Nasalis larvatus	10	0.05	0.38
Pithecia monachus	2	0.02	0.43
Trachypithecus cristatus	18	0.01	0.32
Colobus polykomos	9	0.00	0.36
Macaca fascicularis	6	−0.01	0.33
Presbytis hosei	4	−0.02	0.42
Piliocolobus badius	5	−0.05	0.30
Aotus trivirgatus	8	−0.06	0.29
Galago senegalensis	4	−0.07	0.38
Hapalemur griseus	7	−0.07	0.44
Erythrocebus patas	1	−0.08	0.41
Holocene *Homo sapiens*	**282**	**−0.08**	**0.50**
Cercopithecus mitis	10	−0.12	0.41
Cacajao rubicundus	2	−0.14	0.56
Saimiri sciureus	2	−0.16	0.38
Presbytis rubicunda	5	−0.18	0.39
Macaca mulatta	1	−0.22	0.31
Symphalangus syndactylus	2	−0.23	0.31
Chiropotes satanas	2	−0.25	0.29
Ateles geoffroyi	18	−0.27	0.29
Cebus apella	8	−0.28	0.40
Cebus capucinus	10	−0.36	0.57
Cercocebus torquatus	1	−0.36	0.30
Saimiri oerstedii	1	−0.41	0.41
Miopithecus talapoin	3	−0.49	0.39
Hylobates lar	16	−0.61	0.45

Table 8 (*continued*)

Species (female specimens and fossils only)	*n*	Parietal residual	Parietal diploë ratio
Species (Male specimens and fossils only)	*n*	Parietal residual	Parietal diploë ratio
Alouatta caraya	3	0.78	0.43
Perodicticus potto	5	0.56	0.31
Nycticebus coucang	3	0.53	0.29
Asian *Homo erectus*	**33**	**0.46**	–
Galago alleni	1	0.37	0.32
Australopithecus africanus	**13**	**0.35**	–
Homo heidelbergensis	**17**	**0.28**	–
Paranthropus boisei	**7**	**0.28**	**0.43**
Mandrillus sphinx	1	0.26	0.35
Callithrix argentata	4	0.19	0.43
Propithecus diadema	2	0.19	0.40
African *Homo erectus*	**15**	**0.19**	**0.52**
Callicebus moloch	11	0.19	0.36
Mandrillus leucophaeus	4	0.17	0.46
Papio anubis	6	0.16	0.32
Macaca fuscata	2	0.11	0.30
Theropithecus gelada	1	0.11	0.33
Saguinus midas	6	0.10	0.48
Homo neanderthalensis	**35**	**0.05**	–
Varecia variegata	4	0.04	0.38
Early *Homo*	**13**	**0.03**	**0.52**
Aotus trivirgatus	2	0.00	0.31
Australopithecus afarensis	**8**	**0**	**0.5**
Callithrix humeralifera	2	−0.01	0.44
Pleistocene *Homo sapiens*	**31**	**−0.02**	–
Macaca mulatta	2	−0.04	0.33
Macaca fascicularis	2	−0.08	0.40
Presbytis hosei	1	−0.08	0.30
Pithecia monachus	2	−0.09	0.47
Pithecia pithecia	3	−0.10	0.38
Lophocebus albigena	5	−0.12	0.44
Galago senegalensis	8	−0.15	0.38
Saimiri oerstedii	4	−0.16	0.41
Saimiri sciureus	3	−0.17	0.42
Piliocolobus badius	5	−0.17	0.35
Colobus polykomos	1	−0.19	0.37
Cercocebus torquatus	7	−0.20	0.39
Erythrocebus patas	3	−0.21	0.41
Holocene *Homo sapiens* (males only)	**288**	**−0.21**	**0.48**
Macaca sylvanus	2	−0.23	0.32
Hapalemur griseus	1	−0.23	0.44
Presbytis rubicunda	4	−0.24	0.42
Miopithecus talapoin	3	−0.37	0.33
Propithecus verreauxi	1	−0.46	0.41
Cebus apella	7	−0.48	0.43

analyze the relationship between diploë ratio and *residual* parietal thickness to test whether the thick skulls of hominins are constructed similarly to the skulls of the few extant non-human primates with similarly thick skulls relative to cranial capacity.

Thus, we regressed parietal diploë ratio on residual parietal thickness, as shown in Figures 6 (females only) and 7 (males only). We could then divide the species into four loose groups: those with relatively thick vaults (the vertical line is drawn through the parietal residual value of the species ranked tenth in residual thickness) composed primarily of diploë (diploë ratio > 0.48), those with relatively thick skulls composed primarily of cortical bone, those with relatively thin skulls composed primarily of diploë, and those with relatively thin skulls composed primarily of cortical bone.

The first category (the upper right quadrant in Figures 6 and 7) includes African *H. erectus* and would presumably include Asian *H. erectus* and *Homo heidelbergensis*. While accurate data on the diploë ratio of Asian *H. erectus* and *H. heidelbergensis* are currently unavailable, they are included on the graph as crosses, and the value for their diploë ratio (0.49) is the average of those hominins for which data on diploë ratio are known. In one of the only papers on diploë thickness in *H. erectus* published to date, Balzeau (2006) reports than the diploë makes up 67.4% of the left parietal of Sangiran 17, which provides a small amount of additional support for the placement of Asian *H. erectus* in the upper right quadrant of our Figures 6 and 7 (if we assigned the value of 0.67 to Asian *H. erectus*, it would be above our current y-axis limit, but still remain in the upper right quadrant). Additionally, Weidenreich (1943), stated that all three layers of the cranial vault are thickened in *H. erectus* (*Sinanthropus pekinensis*), but then concluded that the thickening was due to a "peculiar thickening of the outer and inner tables"

(196). A plate in his monograph, however (1943: Figure 20), illustrating a parietal of *Sinanthropus* IV (now Zhoukoudian 4), can be measured, revealing the following relative proportions of the layers: outer table 11.9%, inner table 8.0% and diploë 79.9% (reported in Kennedy [1991]). Thus, we assumed that at least Asian *H. erectus* can safely be placed in the upper right quadrant, and, pending collection of additional data on diploë thickness, felt safe including the other fossil hominins there as well with the caveat that the placement is based on hypothetical ratios.

In the lower right quadrant of Figure 6 (female specimens) are the five non-human primate species with the thickest parietal bones relative to their brain size: *N. coucang*, *P. potto, P. diadema, P. pygmaeus,* and *L. albigena*. Again, *Paranthropus boisei* falls in this quadrant.

In the lower right quadrant of Figure 7 (male specimens) are the five non-human primate species with very thick parietal bones relative to their brain size: *A. caraya*, *P. potto*, *N. coucang*, *G. alleni*, and *M. sphinx*. *Paranthropus boisei* also lies in this quadrant. These six species have thick parietal bones that consist primarily of cortical bone, unlike the fossil hominins in the upper right quadrant.

In the upper left quadrant of both figures lie *A. afarensis*, early *Homo*, and modern humans, all of whom have relatively thin vaults composed primarily of diploë. If Pleistocene *H. sapiens* and Neandertals have a diploë ratio equal to that of an average hominin, they would also fall within this quadrant (they are indicated by the open circles). In Figure 7 (male specimens), only hominins lie in this quadrant. However, several extant non-human primate species represented by female specimens fall within this quadrant in Figure 6, including *Eulemur fulvus*, *Cacajao rubicundus*, *Varecia variegata*, and *Cebus capucinus*, which each have parietal bones that resemble modern humans in terms of their overall relative thickness and high proportion of diploë.

The remaining extant non-human primates fall in the final quadrant and have relatively thin parietal bones composed primarily of cortical bone.

4. Discussion

The results of this study illuminate the questions raised at the start: 1) Is CVT, adjusted for cranial capacity (using residuals), uniquely high in African and Asian *H. erectus* compared to other primates? and 2) Is the composition of African and Asian *H. erectus*, quantified as the ratio of diploë to total thickness, unique among primates?

4.1. Is residual CVT unique in Homo erectus?

Results presented here confirm the general trends reported by Gauld (1992, 1996): total CVT scales with positive allometry to measures of overall size in extant primates. Furthermore, fossil hominins fall above the non-human primate regression line, indicating that they have thicker vault bones than would be expected for a primate of their size. However, some extant species fall well above the regression line as well.

Residual analyses show that African and Asian *H. erectus* do not have significantly higher residual CVT values than several other hominin and extant non-human primate species. Overall, when thickness values adjusted for cranial capacity are compared, *H. erectus* does not have a uniquely thick vault. Several of the extant non-human primate species, such as *A. caraya*, are represented by small sample sizes (in the case of *A. caraya*, a single female and only three male individuals). However, in all analyses, this species is ranked in the top 15 of residual cranial vault thickness (5th in frontal thickness and 13th in parietal thickness using females, and 1st in frontal and parietal thickness using males), suggesting that the pattern is real and should be investigated further. *N. coucang* and *P. potto*, both in the family Lorisidae, were represented by equal numbers of males and females (three each *Nycticebus* and five each *Perodicticus*). *Nycticebus* females ranked 1st in both frontal and parietal residual thickness, while males ranked 2nd in frontal and 3rd in parietal residual thickness. *Perodicticus* females ranked 7th in frontal and 2nd in parietal residual thickness, while the males ranked 10th in frontal and 2nd in parietal thickness. Future research will focus on expanding the available data set of Lorisidae and *Alouatta* CVT to confirm their relative thick-headedness and identify potential causes of it. The comparative method cannot be used to identify the causes of unique features, so the identification of three extant species with potentially similar relative total cranial vault thicknesses as *H. erectus* is important.

Due to potential sexual dimorphism in CVT, the non-human primate sample was divided by sex. While not every species was included in both sex-specific analyses, the overall pattern, suggesting that *H. erectus* does not have uniquely thick cranial vault bones after adjusting for overall size, was similar using either male or female non-human primates. Future studies should increase the sample size of each sex within species, as well as increase the number of species included in each sex-specific analysis in order to more carefully analyze the extant species that appear to resemble *H. erectus* and other hominins in residual CVT.

Our results provide new data on the differences between African and Asian specimens of *H. erectus*. The paleoanthropological community has long been divided on the taxonomic distinction of the fossils that some attribute to a single polytypic species, and others split into two species, generally based on geography. In either case, the Asian specimens have been noted to be more robust overall, with larger cranial capacities, larger cranial superstructures (crests, keels, ridges, eminences), and thicker vaults. Our study, however, provides evidence that African representatives of *H. erectus* have thicker frontal bones relative to brain size than Asian specimens, while the Asian specimens have relatively thicker parietal bones. Our results need confirmation through direct examination of Asian specimens using our photographic technique, as our analyses rely on measures of Asian specimens taken from the literature, compared to a mixture of newly collected data and literature measurements from African specimens. However, if our results are replicated, separation of Asian and African specimens by CVT will not be possible, removing high CVT as a diagnostic feature of a putative Asian clade.

4.2. Is bone composition in Homo erectus unique?

CVT has frequently been considered a simple, single character. However, a single measure of total CVT includes the contributions of the different layers of the cranial vault. There are multiple ways a thick cranial vault can be created——some are composed mainly of cortical bone, while others are predominately diploë. Although diploë ratio was unavailable for many of the hominin specimens, parietal bone composition could be compared among the relatively thick-vaulted *N. coucang*, *A. caraya*, *P. potto*, and *Australopithecus afarensis*, African *H. erectus*, and *Paranthropus boisei*. African *H. erectus* and *A. afarensis* have parietal bones composed of >50% diploë. *Paranthropus boisei* and the extant primate parietal bones are, however, composed of less than 40% diploë. A difference in vault-bone composition is a previously undescribed feature of early hominins.

One problem highlighted by the finding that diploë ratios in humans and some fossil hominins exceed those in non-human primates is that the function of diploë is not known. The distribution of a trilaminar skull form across Vertebrata has never been

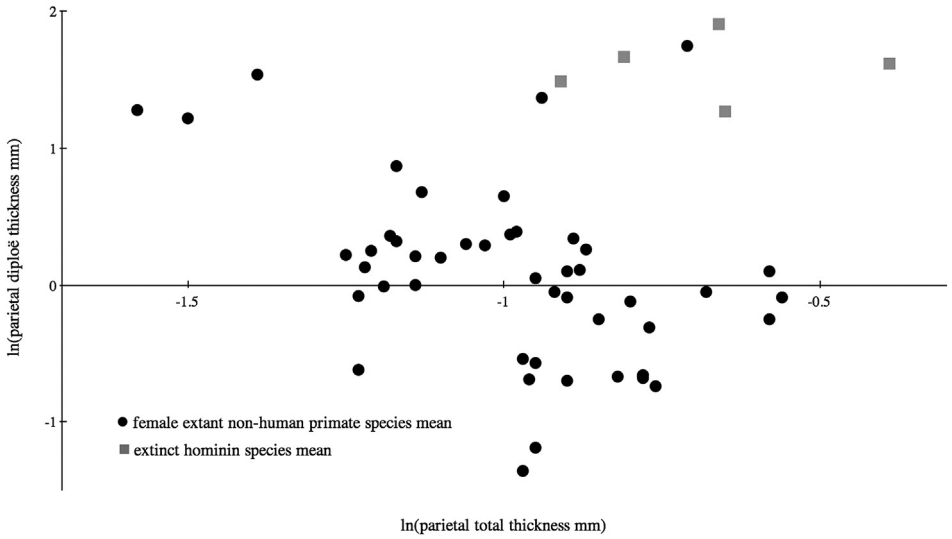

Figure 5. Scatterplot of parietal diploë thickness versus raw parietal thickness using a female non-human primate RMA regression line. Extant female non-human primate species means are represented by black circles; hominin species means are represented by gray squares.

systematically described, but a brief review of CT scans of individuals from 113 vertebrate species from www.digimorph.com revealed intriguing patterns. Only two of nine amphibians and seven of 10 reptiles show three distinct layers, but 15 of 16 birds and 72 of 79 mammals have a distinct trilaminar pattern (SOM Table 7). Most mammals have concentrations of diploë around the sutures, rather than being evenly spread throughout the bones. The largest mammals (elephant, bears, giraffes) have a thick layer of empty space between their external and internal cortical tables, with thin struts connecting the two, but without a true diploë layer. The marine mammals (dolphin, manatee) seem to lack diploë altogether.

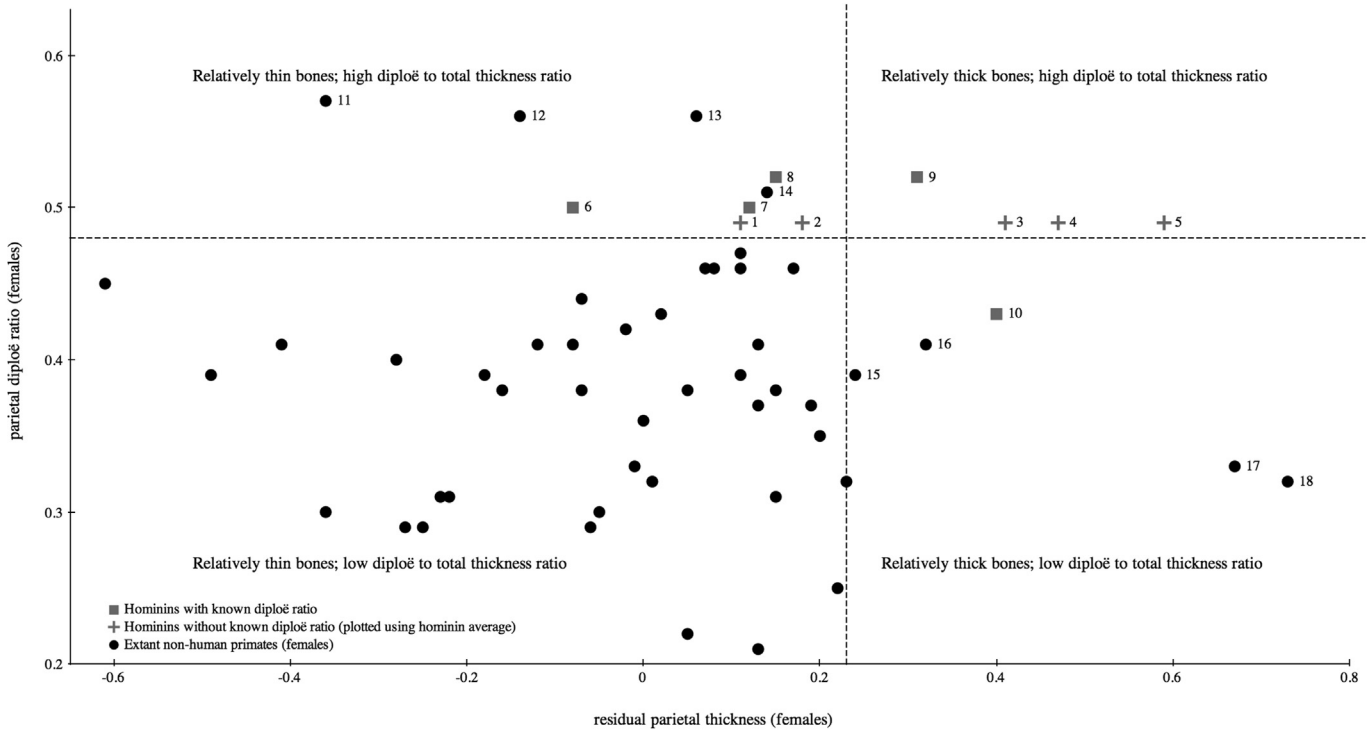

Figure 6. Scatterplot of parietal diploë ratio (diploë: total thickness) versus residual parietal thickness using a female non-human primate RMA regression line. The vertical line (at 0.21) was drawn to separate the 10 species with the highest residual parietal thickness values from the other species. The horizontal line (at 0.48) was drawn to illustrate a natural separation between species with skulls comprised primarily of cortical bone and those with skulls with a higher proportion of diploë. Species for which actual data on diploë thickness are unknown, which are plotted using the hominin mean diploë thickness value (gray crosses): 1. Pleistocene *Homo sapiens*, 2. *Homo neanderthalensis*, 3. *Homo heidelbergensis*, 4. *Australopithecus africanus*. Hominin species for which diploë ratio was collected for the purposes of this study (gray squares): 5. Asian *Homo erectus*, 6. Holocene *Homo sapiens*, 7. *Australopithecus afarensis*, 8. Early *Homo*, 9. African *Homo erectus*, 10. *Paranthropus boisei*. Extant non-human primate species (black circles) that either have particularly high diploë ratios (11–14) or relatively thick parietal bones for their cranial capacity (15–18): 11. *Cebus capucinus*, 12. *Cacajao rubicundus*, 13. *Eulemur fulvus*, 14. *Varecia variegata*, 15. *Pongo pygmaeus*, 16. *Propithecus diadema*, 17. *Perodicticus potto*, 18. *Nycticebus coucang*.

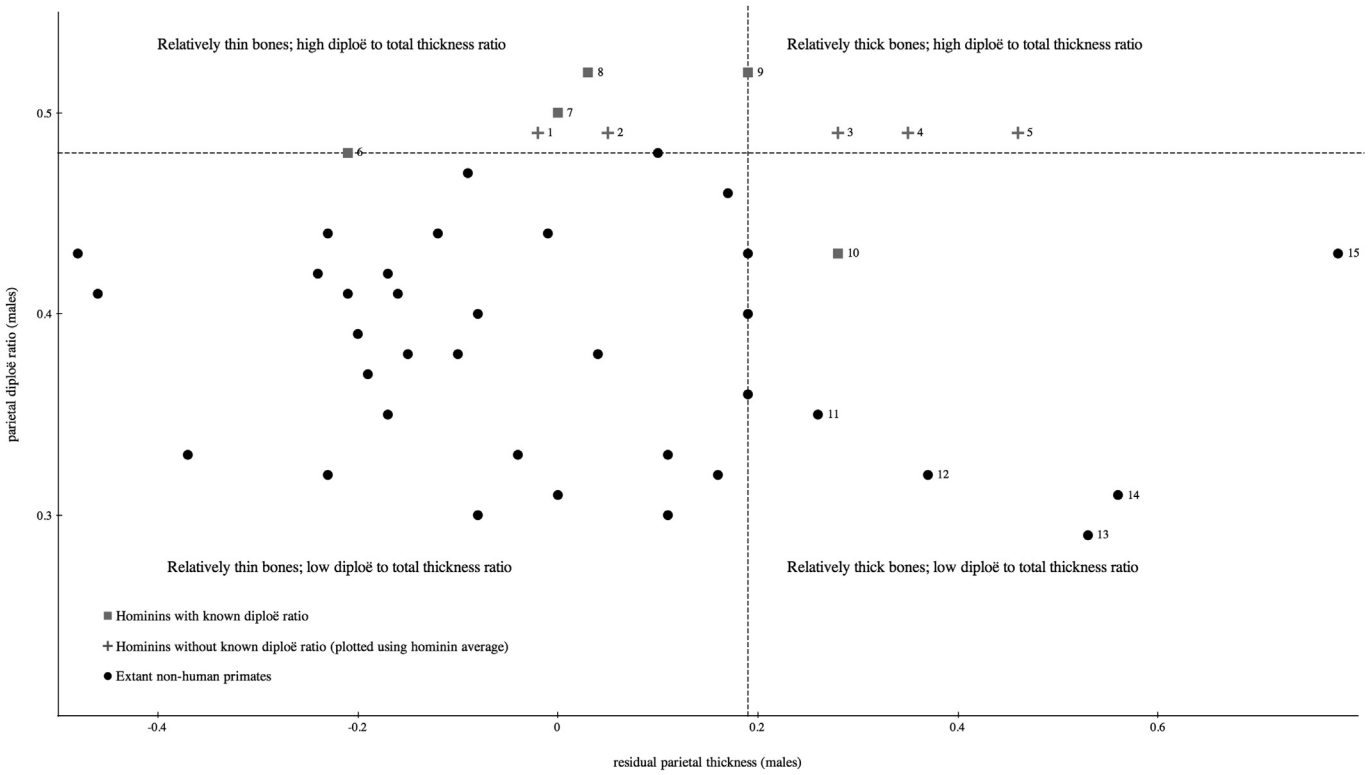

Figure 7. Scatterplot of parietal diploë ratio (diploë: total thickness) versus residual parietal thickness using a male non-human primate RMA regression line. The vertical line (at 0.21) was drawn to separate the ten species with the highest residual parietal thickness values from the other species. The horizontal line (at 0.48) was drawn to illustrate a natural separation between species with skulls comprised primarily of cortical bone and those with skulls with a higher proportion of diploë. Species for which actual data on diploë thickness are unknown, which are plotted using the hominin mean diploë thickness value (gray crosses): 1. Pleistocene *Homo sapiens*, 2. *Homo neanderthalensis*, 3. *Homo heidelbergensis*, 4. *Australopithecus africanus*. Hominin species for which diploë ratio was collected for the purposes of this study (gray squares): 5. Asian *Homo erectus*, 6. Holocene *Homo sapiens*, 7. *Australopithecus afarensis*, 8. Early *Homo*, 9. African *Homo erectus*, 10. *Paranthropus boisei*. Extant non-human primate species that have relatively thick parietal bones for their cranial capacity (black circles): 11. *Mandrillus sphinx*, 12. *Galago alleni*, 13. *Nycticebus coucang*, 14. *Perodicticus potto*, 15. *Alouatta caraya*.

Obviously, an informal visual check for the presence or absence and distribution of diploë across vertebrates can provide no information on other important variables, such as diploic density or mechanical properties. More work is required to determine how different patterns of diploë distribution across the skull affects its structural strength and if variation in diploic density contributes to the overall structural properties of the skull.

It has been suggested that diploë functions to protect the brain by increasing the thickness of the vault while reducing its weight and without proportionally reducing its strength (Anzelmo et al., 2015). While this study was not designed to explicitly test such a hypothesis, our data do allow us to comment on it. Following the biomechanical suggestion, the largest primates in the sample (the great apes) might be expected to demonstrate the highest diploë ratios in order to efficiently reduce the mass of the skull without a concomitant reduction in its strength. Figure 5 suggests that, at least within primates, such a relationship does not exist. Parietal diploë ratios in *Pan* are 0.21 and 0.22, the lowest among all primates. *Gorilla* ratios average 0.25, which is third lowest after the *Pan* species. *Pongo* diploë ratios average 0.39, which ranks 30th of 53 species with known diploë ratios. However, the very low ratios of *Pan* and *Gorilla* suggest that a purely biomechanical explanation may not be sufficient to explain the evolution or function of diploë.

Diploë appears ontogenetically during the "early postnatal" period (Scheuer and Black, 2004), and appears both in bones ossifying intramembranously (i.e., frontal and parietal) and those ossifying endochondrously (i.e., non-squamous occipital). However, diploë itself is considered of dermal intramembranous origin, deriving from neural crest, while cortical bone (even in the frontal and parietal bones) is classified as ossifying via perichondral intramembranous ossification, and is of mesenchymal origin (Scheuer and Black, 2004). Future work on the cell populations of diploë compared to those of cortical vault bone and trabecular bone in long bones is a potentially fruitful area of investigation.

The function, distribution, density, development, and physiology of diploë are certainly avenues left to explore. Given the presumably uniquely high diploë ratios in humans and hominins compared to extant non-human primates, further exploration of diploë is certainly warranted. Our data do allow us to propose that the combination of increased vault thickness and high diploë ratio may be an autapomorphy of at least some mid-Pleistocene hominins, including *H. erectus* and *H. heidelbergensis* (if the diploë ratio of Asian *H. erectus* and *H. heidelbergensis* is confirmed as approximating or exceeding the currently known hominin average).

The dataset compiled for this paper provides the unique opportunity to investigate multiple hypotheses related to cranial vault thickness and composition. Future studies will focus on the allometry of CVT in relation to brain and body size interspecifically among non-human primates and intraspecifically within humans. The data can also be used to empirically test hypotheses related to the responsiveness to CVT to exercise-induced hormonal changes (Lieberman, 1996) and masticatory loading (Menegaz et al., 2010).

5. Conclusions

This research revealed previously unknown variation among extant primates and humans and illustrated that Asian *H. erectus* is

not entirely unique among primates in its cranial vault thickness. The project also identified a possible hominin synapomorphy: high diploë ratios in hominin cranial vault bones compared to those of non-human primates. While a definitive explanation for why and how *H. erectus* grew such thick skulls is still lacking, these new data provide additional clues to this so far intractable paleoanthropological problem.

Acknowledgments

Financial support for this research came from an NSF DDIG #0925793 and a Wenner-Gren dissertation grant to LC. A National Geographic Society fieldwork grant (8827-10) to WHK funded travel to photograph fossils at the National Museums of Kenya and Ethiopia. We thank Emma Mubua and her staff at the National Museums of Kenya, as well as staff at the National Museums of Ethiopia for access to specimens in their care. μCT scanning of the non-human primate sample at Harvard University was made possible with assistance from Lynn Lucas, Fettah Kosar, Judy Chapasko, and Mark Omura. CT scans of humans were obtained during a Smithsonian 10-week summer fellowship to LC with the assistance of Bruno Frohlich, Ian Tattersall, Gisselle Garcia, David Hunt, and Mary Sangrey. Additional measurements of the Point Hope collection were obtained with the help of Jill Shapiro, Dru Munsell, and Nathan Ashe. Richard Feinn provided excellent statistical advice. Gary Schwartz, Mark Spencer, Matt Ravosa, Larry Copes, and Steven Tommasini read and provided invaluable comments on early drafts of this paper. We also thank three anonymous reviewers for their comments, which immensely improved the manuscript.

Supplementary Online Material

Supplementary Online Material related to this article can be found at http://dx.doi.org/10.1016/j.jhevol.2015.08.008

References

Adeloye, A., Kattan, K.R., Silverman, F.N., 1975. Thickness of the normal skull in the American Blacks and Whites. Am. J. Phys. Anthropol. 43, 23–30.
Aiello, L.C., Wood, B.A., 1994. Cranial variables as predictors of hominine body mass. Am. J. Phys. Anthropol. 95, 409–426.
Anderson, R.J., 1882. Observations on the thickness of the human skull. Dublin J. Med. Sci. 74, 270–280.
Andrews, P.J., 1984. An alternative interpretation of the characters used to define *Homo erectus*. Cour. Forsch. Inst. Senckenberg 69, 167–175.
Antón, S.C., 1999. Cranial growth in *Homo erectus*: how credible are the Ngandong juveniles? Am. J. Phys. Anthropol. 108, 223–236.
Antón, S.C., 2002. Evolutionary significance of cranial variation in Asian *Homo erectus*. Am. J. Phys. Anthropol. 118, 301–323.
Antón, S.C., 2003. Natural history of *Homo erectus*. Yrbk. Phys. Anthropol. 46, 126–170.
Antón, S.C., 2004. The face of Olduvai Hominid 12. J. Hum. Evol. 46, 337–347.
Antón, S.C., Spoor, F., Fellmann, C.D., Swisher, C.C., 2007. Defining *Homo erectus*: size considered. In: Henke, W., Tattersall, I. (Eds.), Handbook of Paleoanthropology, Volume 3: Phylogeny of Hominids. Springer, Heidelberg, pp. 1655–1693.
Anzelmo, M., Ventrice, F., Barbeito-Andres, J., Pucciarelli, H.M., Sardi, M.L., 2015. Ontogenetic changes in cranial vault thickness in a modern sample of *Homo sapiens*. Am. J. Hum. Biol. 27, 475–485.
Asfaw, B., 1983. A new hominid parietal from Bodo, Middle Awash Valley. Ethiopia. Am. J. Phys. Anthropol. 61, 367–371.
Balzeau, A., 2006. Are thickened cranial bones and equal participation of the three structural bone layers autpomorphic traits of *Homo erectus*? Bull. Mem. Soc. Anthropologie Paris 18, 145–163.
Balzeau, A., 2013. Thickened cranial vault and parasagittal keeling: correlated traits and autapomorphies of *Homo erectus*? J. Hum. Evol. 64, 631–644.
Behrents, R.G., Carlson, D.S., Abdelnour, T., 1978. *In vivo* analysis of bone strain about the sagittal suture in *Macaca mulatta* during masticatory movements. J. Dent. Res. 57, 904–908.
Bilsborough, A., Wood, B.A., 1988. Cranial morphometry of early hominids: facial region. Am. J. Phys. Anthropol. 76, 61–86.
Bouxsein, M.L., Boyd, S.K., Christiansen, B.A., Guldberg, R.E., Jepsen, K.J., Muller, R., 2010. Guidelines for assessment of bone microstructure in rodents using micro-computed tomography. J. Bone Miner. Res. 25, 1468–1486.
Bräuer, G., Leakey, R.E.F., 1986. The ES-11693 cranium from Eliye Springs, West Turkana, Kenya. J. Hum. Evol. 15, 289–312.
Brown, P., 1994. Cranial vault thickness in Asian *Homo erectus* and *Homo sapiens*. Cour. Forsch. Inst. Senckenberg 171, 33–46.
Byron, C.D., Borke, J., Yu, J., Pashley, D., Wingard, C.J., Hamrick, M., 2004. Effects of increased muscle mass on mouse sagittal suture morphology and mechanics. Anat. Rec. 279, 676–684.
Clarke, R., 1985. A new reconstruction of the Florisbad cranium, with notes on the site. In: Delson, E. (Ed.), Ancestors: The Hard Evidence. Alan R Liss, New York, pp. 301–305.
Copes, L.E., Schwartz, G.T., 2010. The scale of it all: postcanine teeth, the taxon-level effect, and the universality of Gould's scaling law. Paleobiology 36, 188–203.
Day, M.H., Leakey, R.E.F., Walker, A.C., Wood, B.A., 1976. New hominids from East Turkana, Kenya. Am. J. Phys. Anthropol. 45, 369–435.
Day, M.H., Leakey, M.D., Magori, C., 1980. A new hominid fossil skull (L.H. 18) from the Ngaloba Beds, Laetoli, northern Tanzania. Nature 284, 55–56.
Dubois, E., 1937. On the fossil human skulls recently discovered in Java and *Pithecanthropus erectus*. Man 37, 1–7.
Friedland, D.R., Michel, M.A., 2006. Cranial thickness in superior canal dehiscence syndrome: implications for canal resurfacing surgery. Otol. Neurotol. 27, 346–354.
Gauld, S.C., 1992. An allometric study of anthropoid cranial bone thickness: implications for body size estimation in early hominid species. Ph.D. Dissertation, University of California, Los Angeles.
Gauld, S.C., 1996. Allometric patterns of cranial bone thickness in fossil hominids. Am. J. Phys. Anthropol. 100, 411–426.
Getz, B., 1960. Skull thickness in the frontal and parietal regions (a roetgenological examination). Acta Morphol. Neerl-Scand. 3, 221–228.
Hatipoglu, H.G., Ozcan, H.N., Hatipoglu, U.S., Yuksel, E., 2008. Age, sex and body mass index in relation to calvarial diploe thickness and craniometric data on MRI. Forensic Sci. Int. 182, 46–51.
Hwang, K., Kim, J.H., Baik, S.H., 1997. Thickness map of parietal bone in Korean adults. J Craniofac. Surg. 8, 208–212.
Hwang, K., Kim, J.H., Baik, S.H., 1999. The thickness of the skull in Korean adults. J. Craniofac. Surg. 10, 395–399.
Jacob, T., 1973. Paleoanthropological discoveries in Indonesia with special reference to the finds of the last two decades. J. Hum. Evol. 2, 473–485.
Jung, Y.S., Kim, H.J., Choi, S.W., Kang, J.W., Cha, I.H., 2003. Regional thickness of parietal bone in Korean adults. Int. J. Oral Maxillofac. Surg. 32, 638–641.
Kappelman, J., 1996. The evolution of body mass and relative brain size in fossil hominids. J. Hum. Evol. 30, 243–276.
Kennedy, G.E., 1991. On the autapomorphic traits of *Homo erectus*. J. Hum. Evol. 20, 375–412.
Kimbel, W.H., Rak, Y., Johanson, D.C., 2004. The Skull of *Australopithecus afarensis*. Oxford University Press, Oxford.
Lieberman, D.E., 1996. How and why humans grow thin skulls: experimental evidence for systemic cortical robusticity. Am. J. Phys. Anthropol. 101, 217–236.
Lublinsky, S., Ozcivici, E., Judex, S., 2007. An automated algorithm to detect the trabecular-cortical bone interface in micro-computed tomographic images. Calcif. Tissue Int. 81, 285–293.
Lynnerup, N., 2001. Cranial thickness in relation to age, sex and general body build in a Danish forensic sample. Forensic Sci. Int. 117, 45–51.
Lynnerup, N., Astrup, J.G., Sejrsen, B., 2005. Thickness of the human cranial diploe in relation to age, sex and general body build. Head Face Med. 1, 13–19.
Magori, C.C., Day, M.H., 1983. Laetoli Hominid 18: an early *Homo sapiens* skull. J. Hum. Evol. 12, 747–753.
Marsh, H.E., 2013. Beyond thick versus thin: mapping cranial vault thickness patterns in recent *Homo sapiens*. Ph.D. Dissertation, University of Iowa.
McHenry, H.M., 1992. Body size and proportions in early hominids. Am. J. Phys. Anthropol. 87, 407–431.
Menegaz, R.A., Sublett, S.V., Figueroa, S.D., Hoffman, T.J., Ravosa, M.J., Aldridge, K., 2010. Evidence for the influence of diet on cranial form and robusticity. Anat. Rec. 293, 630–641.
Moreira-Gonzalez, A., Papay, F.E., Zins, J.E., 2006. Calvarial thickness and its relation to cranial bone harvest. Plast. Reconstr. Surg. 117, 1964–1971.
Moss, M.L., Young, R.W., 1960. A functional approach to craniology. Am. J. Phys. Anthropol. 18, 281–292.
Nawrocki, S.P., 1991. A biomechanical model of cranial vault thickness in archaic *Homo*. Ph.D. Dissertation, State University of New York.
Peptan, A.I., Lopez, A., Kopher, R.A., Mao, J.J., 2008. Responses of intramembranous bone and sutures upon *in vivo* cyclic tensile and compressive loading. Bone 42, 432–438.
Plavcan, J.M., 2003. Scaling relationships between craniofacial sexual dimorphism and body mass dimorphism in primates: implications for the fossil record. Am. J. Phys. Anthropol. 120, 38–60.
Rawlinson, S.C., Mosley, J.R., Suswillo, R.F., Pitsillides, A.A., Lanyon, L.E., 1995. Calvarial and limb bone cells in organ and monolayer culture do not show the same early responses to dynamic mechanical strain. J. Bone Miner. Res. 10, 1225–1232.
Rightmire, G.P., 1986. Body size and encephalization in *Homo erectus*. Anthropos. (Brno) 23, 823–826.
Roche, A.F., 1953. Increase in cranial thickness during growth. Hum. Biol. 25, 81–92.

Scheuer, L., Black, S., 2004. The Juvenille Skeleton. Elsevier, New York.
Singer, R., 1954. The Saldanha skull from Hopefield, South Africa. Am. J. Phys. Anthropol. 12, 345–362.
Smith, R.J., 2005. Relative size versus controlling for size: misunderstandings about ratios in research on sexual dimorphism in the human corpus collosum. Curr. Anthropol. 46, 249–273.
Smith, R.J., 2009. Use and misuse of the reduced major axis for line-fitting. Am. J. Phys. Anthropol. 140, 476–486.
Tobias, P.V., 1967. Olduvai Gorge. Vol II: The Cranium and Maxillary Dentition of *Australopithecus (Zinjanthropus) boisei*. Cambridge University Press, Cambridge.
Todd, T.W., 1924. Thickness of the male white cranium. Anat. Rec. 27, 245–256.
Walker, A.C., Leakey, R.E.F., 1993. The Nariokotome *Homo erectus* Skeleton. Harvard University Press, Cambridge.
Warton, D.I., Wright, I.J., Falster, D.S., Westoby, M., 2006. Bivariate line-fitting methods for allometry. Biol. Rev. Camb. Philos. Soc. 81, 259–291.
Weidenreich, F., 1943. The Skull of *Sinanthropus pekinensis*: A Comparative Study on a Primitive Hominid Skull. Geological Survey of China, Chungking.
Wood, B.A., 1984. The origin of *Homo erectus*. Cour. Forsch. Sencken. 69, 99–111.